

A flavour GUT model with $\theta_{13}^{\text{PMNS}} \simeq \theta_C/\sqrt{2}$

Stefan Antusch^{*†1}, Christian Gross^{*2}, Vinzenz Maurer^{*3}, Constantin Sluka^{*4}

^{} Department of Physics, University of Basel,
Klingelbergstr. 82, CH-4056 Basel, Switzerland*

*[†] Max-Planck-Institut für Physik (Werner-Heisenberg-Institut),
Föhringer Ring 6, D-80805 München, Germany*

Abstract

We propose a supersymmetric SU(5) GUT model with an A_4 family symmetry – including a full flavon- and messenger sector – which realises the relation $\theta_{13}^{\text{PMNS}} \simeq \theta_C/\sqrt{2}$. The neutrino sector features tri-bimaximal mixing, and $\theta_{13}^{\text{PMNS}} \simeq \theta_C/\sqrt{2}$ emerges from the charged lepton contribution to the PMNS matrix, which in turn is linked to quark mixing via specific GUT relations. These GUT relations arise after GUT symmetry breaking from a novel combination of group theoretical Clebsch-Gordan factors, which in addition to large $\theta_{13}^{\text{PMNS}}$ lead to promising quark lepton mass ratios for all generations of quarks and leptons and to $m_s/m_d = 18.95^{+0.33}_{-0.24}$, in excellent agreement with experimental results. The model also features spontaneous CP violation, with all quark and lepton CP phases determined from family symmetry breaking. We perform a full Markov Chain Monte Carlo fit to the available quark and lepton data, and discuss how the model can be tested by present and future experiments.

¹Email: stefan.antusch@unibas.ch

²Email: christian.gross@unibas.ch

³Email: vinzenz.maurer@unibas.ch

⁴Email: constantin.sluka@unibas.ch

1 Introduction

The longstanding supposition that the mixing angle $\theta_{13}^{\text{PMNS}}$ of the Pontecorvo-Maki-Nakagawa-Sakata (PMNS) matrix U_{PMNS} is possibly not only small but actually vanishing has recently been undone by the data from T2K [1], Double Chooz [2], RENO [3], and in particular Daya Bay [4]. A global fit by the NuFIT collaboration [5] finds $\theta_{13}^{\text{PMNS}} = 8.75^\circ {}^{+0.42^\circ}_{-0.44^\circ}$. This has stimulated a significant amount of interest and excitement in the neutrino flavour physics community.

While one might say that the fact that the reactor angle is not very small does not strengthen the viewpoint that the neutrino masses and mixings are determined by an underlying organising principle, there nevertheless are many interesting open roads for obtaining the neutrino parameters in flavour models. In particular, one may, as e.g. in tri-bimaximal (TBM) mixing models [6], adhere to the assumption that the 1-3 mixing in the neutrino sector, θ_{13}' , is vanishing and that the measured nonzero value of $\theta_{13}^{\text{PMNS}}$ arises from the charged lepton sector only.

This case is especially interesting in the framework of Grand Unified Theories (GUTs) where the Yukawa matrices for the charged leptons and for the down-type quarks have the same origin. One may in that case be tempted to ask whether the fact that $\theta_{13}^{\text{PMNS}}$ agrees well with $\theta_C/\sqrt{2} \simeq 9.2^\circ$ (where θ_C is the Cabibbo angle) is more than a mere coincidence. While it was proposed already many years ago that $\theta_{13}^{\text{PMNS}}$ could/should be of the *order* of the Cabibbo angle (see e.g. [7]), the possibility that the specific relation $\theta_{13}^{\text{PMNS}} \simeq \theta_C/\sqrt{2}$ (up to subleading corrections) emerges out of a realistic GUT has been discussed just recently [8].¹

In Ref. [8], four simple conditions on a flavour GUT model were shown to be sufficient to obtain $\theta_{13}^{\text{PMNS}} \simeq \theta_C/\sqrt{2}$: (i) $\theta_{13}^{\text{PMNS}}$ should arise solely from the 1-2 (and not 1-3) mixing in the charged lepton sector, (ii) the 1-2 mixing in the down quark sector should approximately equal the Cabibbo angle, (iii) the relevant entries in the charged lepton and down quark Yukawa matrices should be generated by a single GUT-operator, and, (iv) the relevant GUT operators should feature certain ratios of Clebsch-Gordan factors (which appear after GUT symmetry breaking in the charged lepton Yukawa matrix). Moreover, it was discussed that – in the case of a supersymmetric (SUSY) SU(5) GUT with vanishing 1-1 element in Y_d and Y_e – only a single combination of the Clebsch factors discussed in [10] is viable, namely $c_{12} = 6$, $c_{21} = -1/2$ and $c_{22} = 6$ (where c_{ij} is the Clebsch of the i-j element of Y_e).²

In this paper we realise these conditions in a specific supersymmetric flavour GUT model. The model is based on a supersymmetric SU(5) GUT with an A_4 family symmetry, supplemented by discrete shaping symmetries and an R -symmetry. The family symmetry is broken by the vacuum expectation values (VEVs) of flavon fields, which – due to an appropriate potential for the flavons – point in specific directions of flavour space and lead to the desired patterns of the Yukawa matrices. Note that, since the Clebsch-Gordan factors play a crucial role for the phenomenological viability of the model, it is essential that we not only provide an effective model valid below the mass scale of messenger fields, but that we also specify the messenger sector.

The model which we construct has, aside from yielding the relation $\theta_{13}^{\text{PMNS}} \simeq \theta_C/\sqrt{2}$,

¹As a phenomenological possibility, the relation $\theta_{13}^{\text{PMNS}} = \theta_C/\sqrt{2}$ was mentioned already some time ago [9]. Its possible origin from charged lepton corrections in Pati-Salam models has been discussed in [10, 11]. In SU(5) GUTs, predictions for large $\theta_{13}^{\text{PMNS}}$ from charged lepton corrections with consistent quark-lepton mass relations were studied in [10, 12], and conditions for realising $\theta_{13}^{\text{PMNS}} = \theta_C/\sqrt{2}$ were given in [8].

²Following a different approach, an SU(5) \times T' model with large $\theta_{13}^{\text{PMNS}}$ close to the current experimental best fit value has been constructed in [13]. Finally, we note that $\theta_{13}^{\text{PMNS}} = \theta_C/\sqrt{2}$ may also be realised in flavour models without quark-lepton unification, as shown in [11].

several additional interesting aspects: First, the angle $\alpha = \arg[-V_{td}V_{tb}^*/(V_{ud}V_{ub}^*)]$ occurring in one of the quark unitarity triangles, which has been measured to be approximately 90° , results not merely from a fit of the model-parameters to the data, but is a built-in feature in that it is a consequence of the so-called quark phase sum rule [14] which holds whenever the 1-3 elements of the quark mass matrices vanish. Second, the CP symmetry is broken only spontaneously due to CP-violating VEVs of the flavon fields. The spontaneous breaking of CP symmetry allows to greatly reduce the fundamental parameters of the model. Finally we obtain an excellent fit for the ratio of the strange- to down-quark mass, which is directly related to the ratio of the muon- to electron-mass and a specific combination of the Clebsch factors mentioned above.

The paper is organised as follows. In section 2, our general strategy for the construction of the flavour model is outlined. The model is then presented in section 3. Subsequently, in section 4, we carefully study its phenomenology and predictions, employing a Markov Chain Monte Carlo (MCMC) analysis, before giving the conclusions of the paper in section 5. The discussion of the superpotential which is responsible for the alignment of the VEVs of the flavon fields, as well as the specification of the renormalizable couplings of the matter-, Higgs-, flavon- and ‘driving’ fields to the messenger fields, is given in the Appendix.

2 Strategy

Before presenting the model in section 3, let us outline the strategy we followed in order to construct it. In the following paragraphs we briefly discuss the general features our model shall have. Afterwards we describe our method to implement these in a concrete model in a consistent way.

General features: Recall that in order to obtain $\theta_{13}^{\text{PMNS}} \simeq \theta_C/\sqrt{2}$ we should have $\theta_{12}^d \simeq \theta_C$, as was discussed in Ref. [8].³ One attractive possibility to realise the latter is to employ quark Yukawa matrices where the 1-3 (left) mixing angles in the down and up sector each vanish and where thus the 1-3 mixing angle of the Cabibbo-Kobayashi-Maskawa (CKM) mixing matrix is generated from 1-2 and 2-3 rotations. The 1-2 mixing angles in the Yukawa matrices can then be expressed in terms of CKM angles and the CKM phase as [14]

$$\theta_{12}^d \simeq \left| \theta_{12}^{\text{CKM}} - \frac{\theta_{13}^{\text{CKM}}}{\theta_{23}^{\text{CKM}}} e^{-i\delta_{\text{CKM}}} \right| \simeq 12.0^\circ \pm 0.3^\circ, \quad \theta_{12}^u \simeq \frac{\theta_{13}^{\text{CKM}}}{\theta_{23}^{\text{CKM}}} \simeq 5.0^\circ \pm 0.3^\circ, \quad (1)$$

such that in particular $\theta_{12}^d \simeq \theta_C$ is realised. Furthermore, under the above assumption of vanishing 1-3 mixings, the quark unitarity triangle angle α is given by the “quark phase sum rule” [14]

$$\alpha \simeq \delta_{12}^d - \delta_{12}^u, \quad (2)$$

which, when fixed to its experimental value of $\sim 90^\circ$, also implies a realistic CKM CP phase δ_{12}^d . In our model, we will predict δ_{12}^d , the phase of the 1-2 mixing in the down-quark sector, to be 90° , via purely real Yukawa matrices except for one single purely imaginary 2-2 entry in Y_d .

In this case, SU(5) relations carry over the CP violation into the lepton sector resulting in a Dirac CP phase $\delta^{\text{PMNS}} = 90^\circ$ as well. Then, the lepton mixing sum rule [15]

$$\theta_{12}^{\text{PMNS}} - \theta_{13}^{\text{PMNS}} \cot(\theta_{23}^{\text{PMNS}}) \cos(\delta^{\text{PMNS}}) \simeq \theta_{12}^\nu, \quad (3)$$

³We use the same notation as in Ref. [14], i.e. the moduli of the complex left-mixing angles of Y_u , Y_d and Y_e are denoted by θ_{ij}^u , θ_{ij}^d and θ_{ij}^e , the associated phases by δ_{ij}^u , δ_{ij}^d and δ_{ij}^e , respectively.

tells us that the PMNS mixing angle $\theta_{12}^{\text{PMNS}}$ does not receive significant corrections to the neutrino mixing angle θ_{12}' . This calls for tri-bimaximal mixing (TBM) ($\theta_{12}' = 35.3^\circ$, $\theta_{23}' = 45^\circ$, $\theta_{13}' = 0$) in the neutrino sector. When the neutrino masses are generated via the type I see-saw mechanism [16], one simple way to obtain TBM is ‘constrained sequential dominance’ [17]. In that scenario, the neutrino masses exhibit a normal mass hierarchy.

In addition to the charged lepton mixing contribution θ_{12}^e , which induces $\theta_{13}^{\text{PMNS}} \simeq \theta_C/\sqrt{2}$ along the lines of [8], our model will also include a charged lepton mixing θ_{23}^e which can generate a deviation of $\theta_{23}^{\text{PMNS}}$ from 45° , as indicated by recent global fits [5, 18].

So how can we obtain Yukawa matrices with the features described above? In our model we generate the rows respectively columns of the Yukawa matrices as VEVs of flavons which are triplets of the family symmetry group A_4 [19]. In App. A we will provide a superpotential for the flavon fields which gives rise to the VEVs used in our model.

A nice feature of our model is that CP symmetry is broken spontaneously by the flavon VEVs.⁴ As was discussed in Ref. [21] (and also briefly in App. A), it is in this way possible to obtain Yukawa matrices which are real except for an imaginary 2-2 element in Y_d and Y_e .

Concerning the GUT flavour structure of our model, we embed the matter content of the Minimal Supersymmetric Standard Model (MSSM) into representations $\mathbf{\bar{5}}$ and $\mathbf{10}$ of $SU(5)$, where the $\mathbf{\bar{5}}$ representation

$$F = (d_R^c \quad d_B^c \quad d_G^c \quad e \quad -\nu) \quad (4)$$

is a triplet under A_4 , whereas the three $\mathbf{10}$ representations are A_4 -invariant singlets

$$T_i = \frac{1}{\sqrt{2}} \begin{pmatrix} 0 & -u_G^c & u_B^c & -u_R & -d_R \\ u_G^c & 0 & -u_R^c & -u_B & -d_B \\ -u_B^c & u_R^c & 0 & -u_G & -d_G \\ u_R & u_B & u_G & 0 & -e^c \\ d_R & d_B & d_G & e^c & 0 \end{pmatrix}_i. \quad (5)$$

Additionally, we introduce, for reasons of minimality, two right-handed neutrinos N_1 and N_2 as invariant singlets under A_4 and $SU(5)$. The $SU(5)$ gauge symmetry is spontaneously broken to the SM gauge group by a VEV of an $SU(5)$ 24-plet H_{24} , while the VEVs of the fields H_5 , $H_{\bar{5}}$ and $H_{\overline{45}}$ lead to electroweak symmetry breaking.⁵

Implementation: To implement the desired features described above, we pursue the following procedure:

- First, we find a suitable set of effective operators for the matter sector together with an appropriate alignment of flavon VEVs, and a superpotential that generates these VEVs.
- The next step is to identify the ‘shaping symmetry’ of the thus specified superpotential. The resulting charges for the fields in our model are given in Table 5 on page 17. Note that this result is not unique as one can redefine the resulting \mathbb{Z}_n symmetries by adding/subtracting the columns of charges of the fields in Table 5.
- Next, one has to come up with a set of messenger fields that, when integrated out, can generate all effective operators. Usually, one has a sizeable freedom of choice in doing

⁴Note that we checked the CP invariance of our superpotential using the ‘generalised’ CP transformation applicable to models with the family group A_4 , cf. [20].

⁵We note that while we will explicitly construct the GUT matter sector and the flavour symmetry breaking sector, the details of the (GUT) Higgs sector are beyond the scope of this paper.

so, both from using different representations for the messengers and from using different ‘topologies’ for the diagrams. For the specific set of messenger fields we choose, see Table 6 on page 18.

- Finally, one has to check whether the identified shaping symmetry allows additional effective operators that can spoil the desired features. If they are non-renormalizable, one can ignore them if they are not actually generated by the specified set of messengers. Otherwise one has to modify some choice made in one of the previous steps, be it the alignment, the structure of the effective superpotential or the set of messenger fields.

Following this procedure, we developed a model where no such dangerous operators are present and which is thus consistent.

3 The Model

We introduce five A_4 triplets called ϕ_i , three A_4 invariant singlets called ξ_i and an A_4 non-invariant singlet in the $\mathbf{1}'$ representation called χ . They break the family symmetry by their VEVs as given in Table 1. A superpotential which induces these VEVs is presented in App. A. The scale Λ is a placeholder for the messenger mass suppression which is specific to that operator which generates the entry (or column respectively row) of the Yukawa matrix (cf. Eqs. (10) and (11)) where the ϵ_i appears. For a full list of the operators, including the messenger fields, which generate the effective superpotential, see the figures on pages 19f.

flavon φ_i :	ϕ_2	ϕ_3	ϕ_{ab}	ϕ_{N_1}	ϕ_{N_2}	ξ_{12}	ξ_{23}	ξ_M	χ
$\frac{\langle \varphi_i \rangle}{\Lambda}$:	$\epsilon_2 \begin{pmatrix} 0 \\ 1 \\ 0 \end{pmatrix}$	$\epsilon_3 \begin{pmatrix} 0 \\ 0 \\ 1 \end{pmatrix}$	$\epsilon_{ab} \begin{pmatrix} c_{ab} \\ -is_{ab} \\ 0 \end{pmatrix}$	$\epsilon_{N_1} \begin{pmatrix} 0 \\ 1 \\ -1 \end{pmatrix}$	$\epsilon_{N_2} \begin{pmatrix} 1 \\ 1 \\ 1 \end{pmatrix}$	ϵ_{12}	ϵ_{23}	ϵ_M	ϵ_χ

Table 1: The VEVs of the flavon fields. The ϵ_i are all assumed to be real numbers. We abbreviated $c_{ab} \equiv \cos(\theta_{ab})$ and $s_{ab} \equiv \sin(\theta_{ab})$.

The effective superpotential in the matter sector is given by⁶

$$W_{\text{eff}} = W_{Y_\nu} + W_{M_R} + W_{Y_d} + W_{Y_u} , \quad (6)$$

with

$$W_{Y_\nu} = (H_5 F)(N_1 \phi_{N_1} + N_2 \phi_{N_2}) , \quad (7a)$$

$$W_{M_R} = \xi_M^2 (N_1^2 \phi_{N_1}^2 + N_2^2 \phi_{N_2}^2) , \quad (7b)$$

$$W_{Y_d} = [T_1 H_{\overline{45}}]_{45} [F H_{24}]_{\overline{45}} \phi_2 + [T_2 H_{24}]_{10} [F H_5]_{\overline{10}} \phi_{ab} \\ + [T_3 H_5]_5 [F H_{24}]_5 \phi_3 + [T_3 H_{24}]_{10} [F H_5]_{\overline{10}} \chi \phi_2 , \quad (7c)$$

$$W_{Y_u} = H_5 (T_3^2 + T_2^2 \phi_{ab}^2 + T_1^2 (\phi_2^2)^2 + T_2 T_3 \xi_{23} + T_1 T_2 \xi_{12}^5) , \quad (7d)$$

⁶For the sake of brevity, we do not explicitly write down the appropriate suppression by powers of the relevant mass scales Λ (which are different for each operator) and we also suppress the couplings in front of each term.

where $[XY]_R$ denotes the contraction of the fields X and Y to an $SU(5)$ tensor in the representation R . When H_{24} obtains its VEV and the GUT symmetry gets broken, Clebsch-Gordan factors, which relate the entries of the charged lepton and down-type quark Yukawa matrices, appear. These factors depend on the way $SU(5)$ indices are contracted and are discrete due to the fact that H_{24} must break $SU(5)$ along the fixed direction of hypercharge. In our model, the Clebsch factors 6, $-1/2$ and $-3/2$,⁷ arise from contractions mediated by $SU(5)$ 10-plet, 45-plet and 5-plet messengers coupling to $H_{\bar{5}}$, $H_{\bar{45}}$ and $H_{\bar{5}}$, respectively, and appear in Y_e (see Eq. (10)). Since we need these specific contractions for our model to work, it is essential that we also construct the messenger sector. The full set of messenger fields, together with their charges, is shown in Table 6 on page 18.

In order to parametrize the resulting Yukawa matrices, we define the quantities⁸

$$\tilde{\epsilon}_i := \frac{\langle H_{24} \rangle}{\Lambda} \epsilon_i \quad \text{and} \quad \hat{\epsilon}_\chi := \frac{\langle H_{24} \rangle \langle \phi_2 \rangle}{\Lambda^2} \epsilon_\chi. \quad (8)$$

We use the convention of the Particle Data Group [23] for the Yukawa matrices after GUT and flavour symmetry breaking

$$W = (Y_u^*)_{ij} Q_i u_j^c H_u + (Y_d^*)_{ij} Q_i d_j^c H_d + (Y_e^*)_{ij} L_i e_j^c H_d + (Y_\nu^*)_{ij} L_i \nu_j^c H_u + (M_\nu^*)_{ij} \nu_i^c \nu_j^c. \quad (9)$$

Up to subleading corrections⁹ the Yukawa matrices of the quarks and charged leptons are then given by

$$Y_d = \begin{pmatrix} 0 & \tilde{\epsilon}_2 & 0 \\ \tilde{\epsilon}_{ab} c_{ab} & i \tilde{\epsilon}_{ab} s_{ab} & 0 \\ 0 & \omega^2 \hat{\epsilon}_\chi & \tilde{\epsilon}_3 \end{pmatrix}, \quad Y_e = \begin{pmatrix} 0 & 6 \tilde{\epsilon}_{ab} c_{ab} & 0 \\ -\frac{1}{2} \tilde{\epsilon}_2 & i 6 \tilde{\epsilon}_{ab} s_{ab} & 6 \omega^2 \hat{\epsilon}_\chi \\ 0 & 0 & -\frac{3}{2} \tilde{\epsilon}_3 \end{pmatrix}, \quad Y_u = \begin{pmatrix} \epsilon_2^4 & \epsilon_{12}^5 & 0 \\ \epsilon_{12}^5 & \epsilon_{ab}^2 & \epsilon_{23} \\ 0 & \epsilon_{23} & y_t \end{pmatrix}, \quad (10)$$

where the complex conjugates of the flavon fields build the rows and columns of the down-type quark and charged lepton Yukawa matrices, respectively. The phase $\omega = \exp(2\pi i/3)$ comes from the fact that the flavon χ transforms as one-dimensional $\mathbf{1}'$ representation of A_4 . The neutrino Yukawa matrix respectively the mass matrix of the heavy neutrinos are given by

$$Y_\nu = \begin{pmatrix} 0 & \epsilon_{N_2} \\ \epsilon_{N_1} & \epsilon_{N_2} \\ -\epsilon_{N_1} & \epsilon_{N_2} \end{pmatrix}, \quad M_R = \begin{pmatrix} M_{R_1} & 0 \\ 0 & M_{R_2} \end{pmatrix}. \quad (11)$$

The mass matrix for the light neutrinos follows from the see-saw formula [16]

$$m_\nu = \frac{v_u^2}{2} Y_\nu M_R^{-1} Y_\nu^T, \quad (12)$$

where $v_u = 246 \text{ GeV} \cdot \sin \beta$. Inserting Eq. (11), we obtain

$$m_\nu = \frac{v_u^2}{2} \begin{pmatrix} A & A & A \\ A & A+B & A-B \\ A & A-B & A+B \end{pmatrix}, \quad \text{with} \quad A = \frac{\epsilon_{N_2}^2}{M_{R_2}}, \quad B = \frac{\epsilon_{N_1}^2}{M_{R_1}}, \quad (13)$$

which implies tri-bimaximal mixing in the neutrino sector. Note that, since m_ν depends only on the two parameters A and B , we are free to fix two of the four parameters which enter Y_ν and M_R , cf. Eq. (15).

⁷More accurately, these are *ratios* of Clebsch factors. For a list and analysis of such ratios, see [22].

⁸Once again we stress that in general specific flavon VEVs do not occur together with a certain messenger field. The suppression of the effective operators by their particular messenger masses and couplings can be obtained from the supergraphs shown in Figures 2–7 on pages 19f.

⁹These could, e.g., stem from higher-dimensional operators or from canonical normalisation [24]. With the messenger sector of the model specified in the Appendix B both corrections can be neglected.

4 Phenomenology

We presented the Yukawa matrices and the mass matrix of the right-handed neutrinos at the GUT scale $M_{\text{GUT}} = 2 \cdot 10^{16}$ GeV. However, to compare with the experimental data, we need the corresponding low energy values, for instance at the mass scale of the top quark $m_t(m_t) = 162.9$ GeV. Besides the renormalization group (RG) running from M_{GUT} to $m_t(m_t)$, one needs to include corrections from supersymmetric thresholds when matching the MSSM to the Standard Model at the superpartner mass scale Λ_{SUSY} . In this section we discuss the inclusion of these effects into our analysis and present a detailed fit of the parameters at M_{GUT} to the observables at $m_t(m_t)$.

4.1 Numerical procedure

The fit is performed in the following way: Using the one-loop MSSM RGEs we run the parameters in the MSSM from M_{GUT} down to $\Lambda_{\text{SUSY}} = 1$ TeV with the Mathematica package REAP [25]. The heavy, right-handed neutrinos are integrated out at their respective mass scales and the effective mass matrix of the light neutrinos is obtained from the see-saw formula. For medium and large $\tan\beta$, SUSY threshold corrections are relevant when matching the MSSM to the Standard Model [26, 27] at Λ_{SUSY} . In our analysis we include the $\tan\beta$ -enhanced SUSY threshold corrections in the basis where Y_u is diagonal with the approximate matching relations at Λ_{SUSY}

$$Y_d^{\text{SM}} = (\mathbf{1} + \text{diag}(\eta_{Q_{12}}, \eta_{Q_{12}}, \eta_{Q_3})) Y_d^{\text{MSSM}} \cos\beta, \quad (14a)$$

$$Y_u^{\text{SM}} = Y_u^{\text{MSSM}} \sin\beta, \quad (14b)$$

$$Y_e^{\text{SM}} = Y_e^{\text{MSSM}} \cos\beta, \quad (14c)$$

where the η_i are proportional to $\tan\beta$. We set $\tan\beta = 40$ to allow for substantial threshold effects, as required for the Clebsch factors 6 and $-3/2$ appearing in our model (cf. [22]). The η_i parameters can be calculated from the sparticle spectrum. Since we do not specify a certain SUSY scenario, we treat them as free parameters in the fit. In a realistic supersymmetry breaking scenario the SUSY threshold corrections for large $\tan\beta$ typically do not exceed about 50% (see e.g. [28]). In the MCMC analysis we therefore implement a prior to restrict the SUSY threshold parameters $\eta_{Q_{12}}$ and η_{Q_3} to values between -0.5 and 0.5 . Note that we have not explicitly included supersymmetric threshold corrections for the charged leptons. They can be absorbed to a good approximation in the quark corrections $\eta_{Q_{12}}$ and η_{Q_3} , since GUTs only predict ratios of quark and charged lepton masses. Finally we evolve the Yukawa matrices from Λ_{SUSY} to $m_t(m_t)$ using the one-loop SM RGEs in REAP, then calculate all observables and compare them to the experimental values. We use the quark- and charged lepton masses at $m_t(m_t)$ given in Ref. [29] for the fit. Although the masses of the charged leptons are given there to high precision, we set their uncertainty to one percent, which is roughly the accuracy of the one-loop calculation used here. The experimental values of $\sin\theta_C$, $\sin\theta_{23}^{\text{CKM}}$, $\sin\theta_{13}^{\text{CKM}}$ and δ^{CKM} are taken from the Winter 2013 fit results of the UTfit collaboration [30]. The lepton mixing observables are fitted to the updated global fit results of the NuFIT collaboration [5].

There are 14 free parameters in our model which we fit: $\tilde{\epsilon}_2, \tilde{\epsilon}_3, \tilde{\epsilon}_{ab}, \theta_{ab}, \hat{\epsilon}_\chi, \eta_{Q_{12}}, \eta_{Q_3}$ for the down-quark and charged-lepton sector and $y_t, \epsilon_{ab}, \epsilon_2, \epsilon_{12}, \epsilon_{23}$ for the up-quark sector.

In the neutrino sector we choose to fix the masses of the right-handed neutrinos

$$Y_\nu = \begin{pmatrix} 0 & \epsilon_{N_2} \\ \epsilon_{N_1} & \epsilon_{N_2} \\ -\epsilon_{N_1} & \epsilon_{N_2} \end{pmatrix}, \quad M_R = 10^{10} \text{ GeV} \cdot \begin{pmatrix} 1 & 0 \\ 0 & 10 \end{pmatrix}, \quad (15)$$

so that the mass matrix of the light neutrinos depends on the parameters ϵ_{N_1} , ϵ_{N_2} . The choice of the right-handed neutrino masses does not significantly affect the fit as long as we are in the regime where the neutrino Yukawa couplings are $\ll 1$.

We perform a global fit of these 14 parameters to the 18 measured observables (9 fermion masses, 3 quark- and 3 lepton mixing angles, the quark mixing phase and the two neutrino mass-squared differences). Having four more observables than parameters implies that our model is capable of predicting four out of these observables. Therefore, including the yet unknown Dirac CP phase δ^{PMNS} and the single physical Majorana phase φ_2^{PMNS} (using the notation as in REAP [25]) of the PMNS matrix in case of a massless lightest neutrino and normal mass hierarchy, our model makes 6 predictions.

4.2 Results

Following the procedure described above, we find a best fit for the parameters with $\chi^2 = 8.1$. Having 14 parameters and 18 fitted observables this translates to a reduced χ^2 of $\chi^2/\text{d.o.f.} = 2.0$. We present the results for the parameters in Table 2.¹⁰ For a discussion of the hierarchy of the ϵ -parameters we refer to Appendix B.

The uncertainty of the results is given as highest posterior density (HPD) intervals. These intervals could be interpreted as Bayesian analogues to the frequentist confidence intervals [23]. The HPD intervals (1σ unless stated otherwise) are obtained from a Markov Chain Monte Carlo (MCMC) analysis, using a Metropolis-Hastings algorithm.

The corresponding best fit values of the observables at m_t are shown in Table 3. Since we used the ‘ \sin^2 ’ of the lepton mixing angles as experimental input for the fit, we also present the values of the lepton mixing parameters in degree in Table 4, for convenience. Correlations among the lepton mixing angles and the Dirac CP phase of the MCMC analysis results are plotted in Figure 1.

4.2.1 Discussion of the results

We now discuss how the results shown in Table 3 and Figure 1 can be understood from analytic formulae and the Yukawa matrices presented in section 3.

Let us start with the prediction for the ratio of m_s and m_d . From our fit, we obtain

$$\frac{m_s}{m_d} = 18.95^{+0.33}_{-0.24}, \quad (16)$$

which is in excellent agreement with the value $m_s/m_d \simeq 18.9 \pm 0.8$ obtained from experiments [31]. In a small angle approximation of the down-type and charged lepton Yukawa matrices one finds to leading order a simple relation between the ratio of the electron- and muon masses, the ratio of the down- and strange-quark masses and the Clebsch-Gordan coefficients (see e.g. [10])

$$\frac{m_s}{m_d} \approx \left| \frac{c_{12}c_{21}}{c_{22}^2} \right| \frac{m_\mu}{m_e}. \quad (17)$$

¹⁰Note that there is a sign ambiguity for the parameters ϵ_2 and ϵ_{ab} , which enter the Yukawa matrix of the up-type quarks at quartic and quadratic order. In our analysis we fix these parameters to be positive.

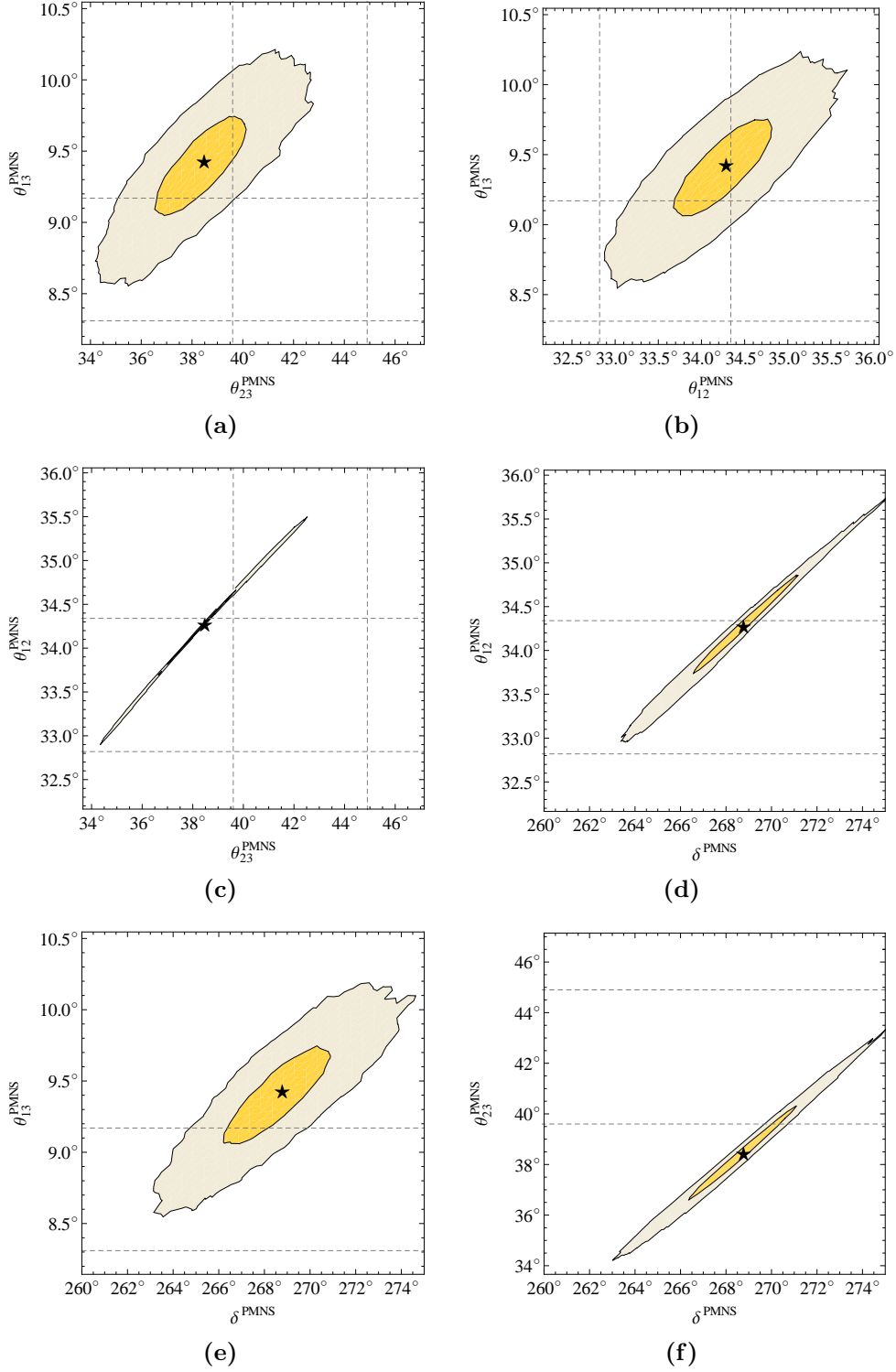


Figure 1: The plots show the correlations among the lepton mixing angles and the Dirac CP phase. The black star marks the best fit value. The yellow and grey regions give the 1σ and 3σ HPD regions obtained from the MCMC analysis, respectively. The dashed grey lines indicate the 1σ intervals for the measured observables.

Parameter	Best fit value	Uncertainty
$\tilde{\epsilon}_2$ in 10^{-4}	6.83	$+0.10$ -0.07
$\tilde{\epsilon}_3$ in 10^{-1}	2.16	± 0.04
$\tilde{\epsilon}_{ab}$ in 10^{-3}	-3.09	$+0.03$ -0.04
θ_{ab}	1.319	$+0.005$ -0.003
$\hat{\epsilon}_\chi$ in 10^{-2}	-1.27	$+0.21$ -0.26
η_{Q12} in 10^{-1}	3.31	$+1.45$ -3.50
η_{Q3} in 10^{-1}	1.93	$+0.49$ -0.38
ϵ_2 in 10^{-2}	$\begin{cases} 5.27 \\ 6.07 \end{cases}$	$\begin{cases} +0.34 \\ -0.36 \\ +0.17 \\ -0.26 \end{cases}$
ϵ_{ab} in 10^{-2}	4.46	$+0.75$ -0.19
ϵ_{12} in 10^{-1}	-1.65	± 0.05
ϵ_{23} in 10^{-2}	1.78	$+0.73$ -0.22
y_t in 10^{-1}	5.29	$+0.29$ -0.25
ϵ_{N1} in 10^{-3}	2.91	± 0.05
ϵ_{N2} in 10^{-3}	3.12	± 0.06

Table 2: Best fit results of the parameters with $\chi^2/\text{d.o.f.} = 2.0$. We give 1σ highest posterior density intervals as uncertainty. The two modes for ϵ_2 can be understood as the two solutions of the (leading order) equation $y_u \approx |(Y_u)_{11} - (Y_u)_{12}^2/(Y_u)_{22}|$, where $(Y_u)_{11} = \epsilon_2^4$.

Although this is just a leading-order estimate, it illustrates well that in order to obtain a valid ratio m_s/m_d , a suitable set of Clebsch factors is mandatory. The Clebsch-Gordan factors of our model, $c_{12} = c_{22} = 6$ and $c_{21} = -1/2$, are in a remarkably good agreement with the experimental data (cf. Eq. (16)).

For comparison, the often used Clebsch coefficients $c_{12} = c_{21} = 1$ and $c_{22} = 3$, leading to the Georgi-Jarlskog relations [32], would result in $m_s/m_d = 25.27$, when considering the 1-2 blocks of Y_e and Y_d with zero 1-1 elements and fitting to the experimental values of θ_C , m_e and m_μ . Note that these Clebsch-Gordan coefficients would also not satisfy the equality condition $c_{12} = c_{22}$ of [8] and therefore predict a too small $\theta_{13}^{\text{PMNS}}$.

The correlations between the lepton mixing parameters, presented in Figure 1, can also be understood from the lepton mixing sum rule $\theta_{12}^{\text{PMNS}} \simeq \theta_{12}^\nu + \theta_{13}^{\text{PMNS}} \cot(\theta_{23}^{\text{PMNS}}) \cos(\delta^{\text{PMNS}})$ and the relation¹¹ $\theta_{13}^{\text{PMNS}} \simeq \theta_C \sin \theta_{23}^{\text{PMNS}}$. The latter relation directly explains the correlation between $\theta_{13}^{\text{PMNS}}$ and $\theta_{23}^{\text{PMNS}}$ in Figure 1a. The correlation between $\theta_{23}^{\text{PMNS}}$ and $\theta_{12}^{\text{PMNS}}$ follows from the lepton mixing sum rule: Larger values of $\theta_{23}^{\text{PMNS}}$ have smaller values of $\cot \theta_{23}^{\text{PMNS}}$. For more than 90% of the MCMC results $\cos(\delta^{\text{PMNS}})$ is negative. Therefore the values of $\theta_{12}^{\text{PMNS}}$ rise with increasing values of $\theta_{23}^{\text{PMNS}}$ as can be seen in Figure 1c. The correlation between $\theta_{12}^{\text{PMNS}}$ and $\theta_{13}^{\text{PMNS}}$ is opposite to what one would naively expect from the lepton mixing sum rule. However one also needs to consider the relation $\theta_{13}^{\text{PMNS}} \simeq \theta_C \sin \theta_{23}^{\text{PMNS}}$, which, when

¹¹There are two effects leading to a deviation from $\theta_{13}^{\text{PMNS}} = \theta_C/\sqrt{2}$. First, the value of $\theta_{23}^{\text{PMNS}} < 45^\circ$ induces $\sin \theta_{23}^{\text{PMNS}} < 1/\sqrt{2}$. Second, our model realises $\theta_{12}^e \gtrsim \theta_C$ which results in a correction to larger values of $\theta_{13}^{\text{PMNS}}$, as discussed in [8].

Observable	Value at m_t	Best fit result	Uncertainty
m_u in MeV	1.22 $^{+0.48}_{-0.40}$	1.22	$^{+0.49}_{-0.40}$
m_c in GeV	0.59 ± 0.08	0.59	± 0.08
m_t in GeV	162.9 ± 2.8	162.89	$^{+2.62}_{-2.36}$
m_d in MeV	2.76 $^{+1.19}_{-1.14}$	2.73	$^{+0.30}_{-0.70}$
m_s in MeV	52 ± 15	51.66	$^{+5.60}_{-13.68}$
m_b in GeV	2.75 ± 0.09	2.75	± 0.09
m_e in MeV	0.485 $\pm 1\%$	0.483	± 0.005
m_μ in MeV	102.46 $\pm 1\%$	102.83	$^{+1.01}_{-0.98}$
m_τ in MeV	1742 $\pm 1\%$	1741.75	$^{+17.38}_{-17.10}$
$\sin \theta_C$	0.2254 ± 0.0007	0.2255	± 0.0007
$\sin \theta_{23}^{\text{CKM}}$	0.0421 ± 0.0006	0.0422	± 0.0006
$\sin \theta_{13}^{\text{CKM}}$	0.0036 ± 0.0001	0.0036	± 0.0001
δ^{CKM} in $^\circ$	69.2 ± 3.1	65.65	$^{+1.78}_{-0.53}$
$\sin^2 \theta_{12}^{\text{PMNS}}$	0.306 ± 0.012	0.317	± 0.006
$\sin^2 \theta_{23}^{\text{PMNS}}$	0.437 $^{+0.061}_{-0.031}$	0.387	$^{+0.017}_{-0.023}$
$\sin^2 \theta_{13}^{\text{PMNS}}$	0.0231 $^{+0.0023}_{-0.0022}$	0.0269	$^{+0.0011}_{-0.0015}$
δ^{PMNS} in $^\circ$	-	268.79	$^{+1.32}_{-1.72}$
φ_2^{PMNS} in $^\circ$	-	297.34	$^{+8.66}_{-10.01}$
Δm_{sol}^2 in 10^{-5} eV^2	7.45 $^{+0.19}_{-0.16}$	7.45	$^{+0.18}_{-0.17}$
Δm_{atm}^2 in 10^{-3} eV^2	2.421 $^{+0.022}_{-0.023}$	2.421	$^{+0.022}_{-0.023}$

Table 3: Best fit results and uncertainties of the observables at $m_t(m_t)$. We give 1σ highest posterior density intervals as uncertainty. Note that although the masses of the charged leptons are known far more precise than listed here, we set an 1% uncertainty for the experimental values, which is roughly the accuracy of the one loop calculation used here.

Observable	Value at m_t	Best fit result	Uncertainty
$\theta_{12}^{\text{PMNS}}$ in $^\circ$	33.57 $^{+0.77}_{-0.75}$	34.29	$^{+0.35}_{-0.39}$
$\theta_{23}^{\text{PMNS}}$ in $^\circ$	41.4 $^{+3.5}_{-1.8}$	38.49	$^{+1.11}_{-1.26}$
$\theta_{13}^{\text{PMNS}}$ in $^\circ$	8.75 $^{+0.42}_{-0.44}$	9.43	$^{+0.20}_{-0.25}$

Table 4: Best fit results for the lepton mixing angles at $m_t(m_t)$, given here in degree for convenience.

plugged into the lepton mixing sum rule leads to

$$\theta_{12}^{\text{PMNS}} \simeq \theta_{12}^\nu - \theta_C \sqrt{1 - (\theta_{13}^{\text{PMNS}})^2 / \theta_C^2} \left| \cos(\delta^{\text{PMNS}}) \right|, \quad (18)$$

where the negative sign of $\cos \delta^{\text{PMNS}}$ is written explicitly. This explains the rising of $\theta_{12}^{\text{PMNS}}$ with increasing $\theta_{13}^{\text{PMNS}}$ seen in Figure 1b. The correlation in Figure 1d is again obvious from the lepton mixing sum rule. Naively one would not expect correlations between δ^{PMNS} and the lepton mixing angles $\theta_{13}^{\text{PMNS}}$ and $\theta_{23}^{\text{PMNS}}$, respectively. The correlations seen in Figures 1e and 1f however follow indirectly from the other correlations discussed above.

4.2.2 Testability of the model

Finally, we point out predictions which may allow to falsify the model:

- We find best fit values of $\theta_{13}^{\text{PMNS}} = 9.44^\circ_{-0.25^\circ}^{+0.20^\circ}$ and $\theta_{23}^{\text{PMNS}} = 38.49^\circ_{-1.26^\circ}^{+1.11^\circ}$, which lie within the respective 2σ intervals reported in [5]. Future, more precise measurements of $\theta_{13}^{\text{PMNS}}$ and $\theta_{23}^{\text{PMNS}}$ therefore have the potential to falsify our model.
- For the yet unmeasured Dirac CP phase of the PMNS matrix we predict $\delta^{\text{PMNS}} = 268.79^\circ_{-1.72^\circ}^{+1.32^\circ}$.
- From the prediction of δ^{PMNS} follows that the $\cos \delta^{\text{PMNS}}$ term in the lepton mixing sum rule leads to a negative correction to the TBM prediction of 35.3° for the solar mixing angle. We find $\theta_{12}^{\text{PMNS}} = 34.29^\circ_{-0.40^\circ}^{+0.35^\circ}$. This is still slightly larger than what is currently reported from experiments. However, from Figure 1c one can deduce that if, as our model predicts, smaller values of $\theta_{23}^{\text{PMNS}}$ will be observed, the solar mixing angle will comply with experiments.
- In the quark sector, we predict a CKM phase $\delta^{\text{CKM}} = 65.65^\circ_{-0.53^\circ}^{+1.78^\circ}$. This is a slight discrepancy with the experimental value of $69.2^\circ \pm 3.1^\circ$, so that a future more precise determination of δ^{CKM} could falsify our model. As already discussed in Eq. (16) the model predicts $m_s/m_d = 18.95_{-0.24}^{+0.33}$, which is currently in excellent agreement with experiments, but will be tested further in the future.
- Our prediction for the Majorana phase $\varphi_2^{\text{PMNS}} = 297.34^\circ_{-10.01^\circ}^{+8.66^\circ}$ is extremely difficult to be tested, because – due to the normal hierarchy of neutrino masses – the effective mass parameter which is determined in neutrino-less double beta decay experiments is

$$m_{\beta\beta} = \left| (U_{e2}^{\text{PMNS}})^2 \sqrt{\Delta m_{\text{sol}}^2} + (U_{e3}^{\text{PMNS}})^2 \sqrt{\Delta m_{\text{atm}}^2} \right| = (2.31_{-0.09}^{+0.12}) \cdot 10^{-3} \text{ eV}, \quad (19)$$

which is far below the sensitivity of current experiments. Of course, if an inverse hierarchy would be measured, the model would be falsified.

5 Summary and conclusions

Motivated by the possibility that the good agreement between $\theta_{13}^{\text{PMNS}}$ and $\theta_C/\sqrt{2}$ is no coincidence, we have proposed a first supersymmetric flavour GUT model with SU(5) GUT symmetry and A_4 family symmetry, where this relation is realised. Based on one of the strategies discussed in [8], the neutrino sector of our model features tri-bimaximal mixing, and $\theta_{13}^{\text{PMNS}} \simeq \theta_C/\sqrt{2}$ emerges from the charged lepton contribution to the PMNS matrix, which

in turn is linked to quark mixing via specific GUT relations. We explicitly constructed the GUT matter sector of the model, including the full flavon and messenger sectors.

The model has several remarkable properties: For instance, the GUT mixing relations leading to $\theta_{13}^{\text{PMNS}} \simeq \theta_C/\sqrt{2}$ arise after GUT symmetry breaking from a novel combination of group theoretical Clebsch factors, namely $c_{12} = c_{22} = 6$ and $c_{21} = -1/2$, which are in excellent agreement with the current experimental data for m_s/m_d (cf. Eq. (16)). Furthermore, CP symmetry is broken spontaneously by the VEVs of the flavon fields in a way that the angle α of the quark unitary triangle is close to 90° (implying a consistent quark CP phase δ^{CKM}). This way, also the CP phases of the neutrino sector are predicted, with close-to-maximal CP violation $\delta^{\text{PMNS}} \approx 270^\circ$.

Taking into account the RG-evolution of the parameters between the GUT-scale and the electroweak scale, as well as supersymmetric threshold corrections, we have performed a detailed fit of the 14 model parameters to the 18 measured observables. We find a good best-fit point with a $\chi^2/\text{d.o.f.}$ of 2.0. We have also performed a full Markov Chain Monte Carlo fit from which we derive the highest posterior density 1σ intervals for all parameters and observables. With 14 parameters and 18 measured observables plus the PMNS Dirac phase and one Majorana phase, the model features 6 predictions, and we have discussed how these can be tested by present and future experiments.

Acknowledgements

This project was supported by the Swiss National Science Foundation (projects 200021-137513 and CRSII2-141939-1).

Appendix

A The flavon superpotential

Here we present the mechanism responsible for the vacuum alignment of the A_4 -triplet flavons ϕ_i , the A_4 -invariant flavons ξ_i and the flavon χ in the $\mathbf{1}'$ representation. The scalar potential for the flavons is obtained from the F -term contributions of the ‘driving fields’ S, D, A and O which have R -charge 2. Supersymmetric minima occur when the F -terms vanish. All flavons and driving fields are listed in the lower part of Table 5 together with their charges under the imposed symmetries. Note that the S -fields are all singlets with respect to all symmetries (apart from R -symmetry) and hence are interchangeable.

The total effective (i.e. after integrating out the messenger fields) superpotential which is responsible for the vacuum alignment of the flavons, see Table 1, is given by

$$W_{\text{flavon}} = W_{\perp} + W_{ab} + W_{N_1 N_2} + W_{\chi} + W_M + W_{12} \quad (20)$$

where^{12,13}

$$W_{\perp} = S_2[(\phi_2^2)^3 - M_2^2] + S_3[\phi_3^2 - M_3^2] + A_2(\phi_2 \star \phi_2) + A_3(\phi_3 \star \phi_3) + O_{2,3}(\phi_2 \phi_3), \quad (21a)$$

¹²As we did for the matter-superpotential, we omit the appropriate suppressions by powers of the messenger masses.

¹³We use the Ma-Rajasekaran (“ $SO(3)$ -like”) basis for A_4 in this work, as introduced in the first reference of [19]. The singlet of $\mathbf{3} \otimes \mathbf{3}$ is given by the $SO(3)$ -type inner product. There are two $\mathbf{3}$ ’s in $\mathbf{3} \otimes \mathbf{3}$, constructed from the antisymmetric cross-product (\times) and the symmetric star-product (\star), respectively. The brackets $(\dots)_{1'}$ and $(\dots)_{1''}$ mean that the fields are contracted to the $\mathbf{1}'$ and $\mathbf{1}''$ representation of A_4 , respectively.

$$W_{ab} = S_{ab}[(\phi_{ab} \star \phi_{ab})^2 \xi_{23}^2 - M_{ab}^2] + D_{ab}^\alpha [\phi_{ab}^2 + \lambda_{ab} \xi_{23}^2] + D_{ab}^\beta (\phi_{ab} \star \phi_{ab}) \phi_{ab} + D_{ab}^\gamma [(\phi_{ab}^2)_{1'} (\phi_{ab}^2)_{1''} + k_{ab} (\phi_{ab} \star \phi_{ab})^2], \quad (21b)$$

$$W_{N_1 N_2} = S_{N_1}[(\phi_{N_1} \star \phi_{N_1})^2 \phi_{N_1}^2 - M_{N_1}^2] + D_{N_1}(\phi_{N_1} \star \phi_{N_1}) \phi_{N_1} + O_{N_1; N_2}(\phi_{N_1} \phi_{N_2}) + S_{N_2}[(\phi_{N_2}^2)^3 - M_{N_2}^2] + D'_{N_2}(\phi_{N_2}^2)_{1''} + D''_{N_2}(\phi_{N_2}^2)_{1'}, \quad (21c)$$

$$W_\chi = S_\chi[\chi^6 - M_\chi^2], \quad (21d)$$

$$W_M = S_M[\xi_M^6 - M_M^2], \quad (21e)$$

$$W_{12} = S_{12}[\xi_{12}^6 - M_{12}^2]. \quad (21f)$$

Recall that the constants M^2 are real due to the unbroken CP symmetry. The first terms of each part, which are of the form $S(\varphi^n - M^2)$, restrict the phases of the flavon VEVs to specific discrete values. In particular, among the discrete vacua for the phases we have 0° and 180° for n even and $M^2 > 0$, which we assume everywhere in Eq. (21). Hence, up to a discrete choice, one obtains the real VEVs for χ , ξ_M and ξ_{12} , see Table 1. Let us now briefly discuss the three remaining parts W_\perp , W_{ab} and $W_{N_1 N_2}$ in the following:

W_\perp : The terms with the triplet driving fields A_i force two of each $\langle \phi_i \rangle$'s components to vanish and the term with the driving field $O_{2;3}$ forces $\langle \phi_2 \rangle$ and $\langle \phi_3 \rangle$ to be orthogonal. Therefore, W_\perp has supersymmetric minima at the points $\langle \phi_2 \rangle$ and $\langle \phi_3 \rangle$ specified in Table 1.

W_{ab} : The term with the singlet driving field S_{ab} determines the magnitude of the *product* of $\langle \phi_{ab} \rangle \langle \xi_{23} \rangle$ and its overall phase by the mechanism explained above. The *individual* magnitudes and the relative phase between $\langle \phi_{ab} \rangle$ and $\langle \xi_{23} \rangle$ are determined by the F -term of D_{ab}^α . The term with the driving field D_{ab}^β sets one of the components of $\langle \phi_{ab} \rangle$ to zero. While the overall phase and norm of $\langle \phi_{ab} \rangle$ are already fixed by the F -terms of S_{ab} and D_{ab}^α , the relative magnitude and phase of the two non-vanishing components are fixed by the F -term of D_{ab}^γ . Depending on the value of k_{ab} there are three distinct solutions for these remaining components: For $-1 \leq k_{ab} \leq 3$ the moduli of the two non-vanishing components are equal, while their relative phase φ is given by $k_{ab} = 1 - 2\cos(2\varphi)$. Defining the ratio of the moduli of the two non-vanishing components as $\tan\theta_{ab}$, the other two solutions are given by $\varphi \in \{0, \pi\}$, $k_{ab} = -1 - 4\cot^2(2\theta_{ab})$ for $k_{ab} < -1$ and $\varphi = \pm\frac{\pi}{2}$, $k_{ab} = 3 + 4\cot^2(2\theta_{ab})$ for $k_{ab} > 3$, respectively. With an appropriate choice of k_{ab} the potential has a minimum at the points $\langle \phi_{ab} \rangle$ and $\langle \xi_{23} \rangle$ given in Table 1.

$W_{N_1 N_2}$: One can easily check that the second line of $W_{N_1 N_2}$ has a supersymmetric minimum at $\langle \phi_{N_2} \rangle \propto (1, 1, 1)^T$. The term with the driving field D_{N_1} in the first line sets one of the components of $\langle \phi_{N_1} \rangle$ to zero. Finally, the orthogonality condition between $\langle \phi_{N_1} \rangle$ and $\langle \phi_{N_2} \rangle$, which results from setting to zero the F -term of $O_{N_1; N_2}$, leads to $\langle \phi_{N_1} \rangle \propto (0, 1, -1)^T$, cf. Table 1.

B The messenger sector

In this appendix we elaborate on the set of heavy messenger fields that, when integrated out, give rise to the effective superpotentials of Section 3 and Appendix A. As discussed in Section 2, in order not to generate undesired effective operators the messenger sector has to be selected carefully. Note that the choice of the messenger sector is not unique. In the following we present the messenger fields Φ_i and $\bar{\Phi}_i$, the supergraphs that give rise to

the effective operators and discuss that the numerical values for the ϵ -parameters defined in Eqs. (10) and (11) can be obtained with a suitable choice for the masses of the messenger fields.

The quantum numbers of half of the messenger fields Φ_i are explicitly shown in Table 6. For each field Φ_i there is a corresponding field $\bar{\Phi}_i$ with ‘opposite’ quantum numbers, i.e. quantum numbers such that a mass term $\Lambda_i \Phi_i \bar{\Phi}_i$ is allowed in the superpotential.

In Figures 2–7 on pages 19f we show the supergraphs that lead to the effective operators when the messenger fields are integrated out. Each supergraph topology in Figures 2–6 corresponds to several operators, which are shown in the table below each graph. In each of the supergraphs, the external fields, which can be either matter-, Higgs-, flavon- or driving-fields, are labeled by φ_i , whereas the messenger fields are labeled by γ_i and $\bar{\gamma}_i$. Note that many of the messenger fields occur in more than one operator.

Finally let us comment on the consistency of the different orders of magnitude for the numerical values of the ϵ -parameters in Table 2. They arise as effective couplings after integrating out the heavy messenger fields and inserting the vevs for the flavon fields and the GUT-Higgs field in the corresponding non-renormalizable operators. As can be checked from Figures 2–7 on pages 19f the different orders of magnitude of the parameters, which are needed to fit the data, can originate from an appropriate choice for the masses of the individual messenger fields which appear in the corresponding effective operators. Let us consider the parameters $\tilde{\epsilon}_2$, $\tilde{\epsilon}_3$ and $\hat{\epsilon}_\chi$ as an example. Up to messenger couplings which may be assumed to be $\mathcal{O}(1)$, they are given by

$$\tilde{\epsilon}_2 = \frac{\langle H_{24} \rangle \langle \phi_2 \rangle}{\Lambda_6 \Lambda_7}, \quad \tilde{\epsilon}_3 = \frac{\langle H_{24} \rangle \langle \phi_3 \rangle}{\Lambda_{10} \Lambda_{11}}, \quad \hat{\epsilon}_\chi = \frac{\langle H_{24} \rangle \langle \phi_2 \rangle \langle \chi \rangle}{\Lambda_{32} \Lambda_{33} \Lambda_{34}}. \quad (22)$$

These messenger mass scales are specific to these parameters and therefore the hierarchy $|\tilde{\epsilon}_2| \ll |\hat{\epsilon}_\chi| \ll |\tilde{\epsilon}_3|$ can arise from a hierarchy of $\Lambda_{10} \Lambda_{11} \ll \Lambda_{32} \Lambda_{33} \Lambda_{34} / \langle \chi \rangle \ll \Lambda_6 \Lambda_7$. Similar arguments hold for the other parameters.

References

- [1] K. Abe *et al.* [T2K Collaboration], Phys. Rev. Lett. **107** (2011) 041801 [arXiv:1106.2822 [hep-ex]].
- [2] Y. Abe *et al.* [DOUBLE-CHOOZ Collaboration], Phys. Rev. Lett. **108** (2012) 131801 [arXiv:1112.6353 [hep-ex]].
- [3] J. K. Ahn *et al.* [RENO Collaboration], Phys. Rev. Lett. **108** (2012) 191802 [arXiv:1204.0626 [hep-ex]].
- [4] F. P. An *et al.* [DAYA-BAY Collaboration], Phys. Rev. Lett. **108** (2012) 171803 [arXiv:1203.1669 [hep-ex]]; F. P. An *et al.* [DAYA-BAY Collaboration], Chin. Phys. C **37** (2013) 011001 [arXiv:1210.6327 [hep-ex]].
- [5] M. C. Gonzalez-Garcia, M. Maltoni, J. Salvado and T. Schwetz [NuFIT Collaboration], JHEP **1212** (2012) 123 [arXiv:1209.3023 [hep-ph]], NuFIT 1.1 (2013) updated fit results available at www.nu-fit.org
- [6] P. F. Harrison, D. H. Perkins and W. G. Scott, Phys. Lett. B **530** (2002) 167 [hep-ph/0202074].

- [7] F. Vissani, JHEP **9811** (1998) 025 [hep-ph/9810435]; F. Vissani, Phys. Lett. B **508** (2001) 79 [hep-ph/0102236]; P. Ramond, Int. J. Mod. Phys. A **20** (2005) 1234 [hep-ph/0405176]; A. Datta, L. Everett and P. Ramond, Phys. Lett. B **620** (2005) 42 [hep-ph/0503222]; L. L. Everett, Phys. Rev. D **73** (2006) 013011 [hep-ph/0510256]; Y.-L. Wu, Phys. Lett. B **714** (2012) 286 [arXiv:1203.2382 [hep-ph]].
- [8] S. Antusch, C. Gross, V. Maurer and C. Sluka, Nucl. Phys. B **866** (2013) 255 [arXiv:1205.1051 [hep-ph]].
- [9] See e.g.: H. Minakata and A. Y. Smirnov, Phys. Rev. D **70** (2004) 073009 [hep-ph/0405088].
- [10] S. Antusch and V. Maurer, Phys. Rev. D **84** (2011) 117301 [arXiv:1107.3728 [hep-ph]].
- [11] S. F. King, Phys. Lett. B **718** (2012) 136 [arXiv:1205.0506 [hep-ph]].
- [12] D. Marzocca, S. T. Petcov, A. Romanino and M. Spinrath, JHEP **1111** (2011) 009 [arXiv:1108.0614 [hep-ph]].
- [13] A. Meroni, S. T. Petcov and M. Spinrath, Phys. Rev. D **86** (2012) 113003 [arXiv:1205.5241 [hep-ph]].
- [14] S. Antusch, S. F. King, M. Malinsky and M. Spinrath, Phys. Rev. D **81** (2010) 033008 [arXiv:0910.5127 [hep-ph]].
- [15] S. F. King, JHEP **0508** (2005) 105 [arXiv:hep-ph/0506297]; I. Masina, Phys. Lett. B **633** (2006) 134 [arXiv:hep-ph/0508031]; S. Antusch and S. F. King, Phys. Lett. B **631** (2005) 42 [hep-ph/0508044]; S. Antusch, P. Huber, S. F. King and T. Schwetz, JHEP **0704** (2007) 060 [arXiv:hep-ph/0702286].
- [16] P. Minkowski, Phys. Lett. B **67** (1977) 421; M. Gell-Mann, P. Ramond and R. Slansky in Sanibel Talk, CALT-68-709, Feb 1979, and in *Supergravity* (North Holland, Amsterdam 1979); T. Yanagida in *Proc. of the Workshop on Unified Theory and Baryon Number of the Universe*, KEK, Japan, 1979; S.L.Glashow, Cargese Lectures (1979); R. N. Mohapatra and G. Senjanovic, Phys. Rev. Lett. **44** (1980) 912; J. Schechter and J. W. Valle, Phys. Rev. D **25** (1982) 774.
- [17] S. F. King, JHEP **0209** (2002) 011 [hep-ph/0204360].
- [18] G. L. Fogli, E. Lisi, A. Marrone, A. Palazzo and A. M. Rotunno, Phys. Rev. D **84** (2011) 053007 [arXiv:1106.6028 [hep-ph]].
- [19] For early works on A_4 family symmetry models, see e.g.: E. Ma and G. Rajasekaran, Phys. Rev. D **64** (2001) 113012 [hep-ph/0106291]; K. S. Babu, E. Ma and J. W. F. Valle, Phys. Lett. B **552** (2003) 207 [hep-ph/0206292]; G. Altarelli and F. Feruglio, Nucl. Phys. B **720** (2005) 64 [hep-ph/0504165].
- [20] F. Feruglio, C. Hagedorn and R. Ziegler, arXiv:1211.5560 [hep-ph]; M. Holthausen, M. Lindner and M. A. Schmidt, JHEP **1304** (2013) 122 [arXiv:1211.6953 [hep-ph]].
- [21] S. Antusch, S. F. King, C. Luhn and M. Spinrath, Nucl. Phys. B **850** (2011) 477 [arXiv:1103.5930 [hep-ph]].
- [22] S. Antusch and M. Spinrath, Phys. Rev. D **79** (2009) 095004 [arXiv:0902.4644 [hep-ph]].

- [23] J. Beringer *et al.* [Particle Data Group Collaboration], Phys. Rev. D **86** (2012) 010001.
- [24] S. Antusch, S. F. King, M. Malinsky, JHEP **0805** (2008) 066. [arXiv:0712.3759 [hep-ph]]; S. Antusch, S. F. King and M. Malinsky, Phys. Lett. B **671** (2009) 263 [arXiv:0711.4727 [hep-ph]]; M. -C. Chen, M. Fallbacher, M. Ratz and C. Staudt, Phys. Lett. B **718** (2012) 516 [arXiv:1208.2947 [hep-ph]]; M. -C. Chen, M. Fallbacher, Y. Omura, M. Ratz and C. Staudt, Nucl. Phys. B **873** (2013) 343 [arXiv:1302.5576 [hep-ph]].
- [25] S. Antusch, J. Kersten, M. Lindner, M. Ratz and M. A. Schmidt, JHEP **0503** (2005) 024 [arXiv:hep-ph/0501272].
- [26] L. J. Hall, R. Rattazzi and U. Sarid, Phys. Rev. D **50** (1994) 7048 [arXiv:hep-ph/9306309]; M. S. Carena, M. Olechowski, S. Pokorski and C. E. M. Wagner, Nucl. Phys. B **426** (1994) 269 [arXiv:hep-ph/9402253]; R. Hempfling, Phys. Rev. D **49** (1994) 6168.
- [27] T. Blazek, S. Raby and S. Pokorski, Phys. Rev. D **52** (1995) 4151 [arXiv:hep-ph/9504364].
- [28] S. Antusch and M. Spinrath, Phys. Rev. D **78** (2008) 075020 [arXiv:0804.0717 [hep-ph]].
- [29] Z. Z. Xing, H. Zhang and S. Zhou, Phys. Rev. D **77** (2008) 113016 [arXiv:0712.1419 [hep-ph]].
- [30] M. Bona *et al.* [UTfit Collaboration], JHEP **0507** (2005) 028 [arXiv:hep-ph/0501199], Winter 2013 (pre-Moriond13) updated fit results available at www.utfit.org/UTfit/ResultsWinter2013PreMoriond.
- [31] H. Leutwyler, Phys. Lett. B **378** (1996) 313 [hep-ph/9602366].
- [32] H. Georgi and C. Jarlskog, Phys. Lett. B **86** (1979) 297.

	SU(5)	A_4	$\mathbb{Z}_2^{(a)}$	$\mathbb{Z}_2^{(b)}$	$\mathbb{Z}_6^{(a)}$	$\mathbb{Z}_6^{(b)}$	$\mathbb{Z}_6^{(c)}$	$\mathbb{Z}_6^{(d)}$	$\mathbb{Z}_6^{(e)}$	$U(1)_a$	$U(1)_b$	$U(1)_R$
Matter Fields												
F	$\bar{\mathbf{5}}$	$\mathbf{3}$.	.	.	4	4	.	.	.	2	1
T_1	$\mathbf{10}$	1	1
T_2	$\mathbf{10}$.	.	.	1	.	4	.	.	.	1	1
T_3	$\mathbf{10}$.	1	.	.	.	2	.	.	.	1	1
N_1	2	2	1	.	.	.	1
N_2	2	2	1	1	.	.	1
Higgs Fields												
H_5	$\mathbf{5}$	2	.	.	.	-2	.
$H_{\bar{5}}$	$\bar{\mathbf{5}}$.	.	1	.	2	.	.	.	-1	.	.
H_{45}	$\mathbf{45}$	4	5	.	.	1	.	2
$H_{\bar{45}}$	$\bar{\mathbf{45}}$	2	1	.	.	-1	.	.
H_{24}	$\mathbf{24}$	1	-3	.
Flavon Fields												
ϕ_2	.	$\mathbf{3}$	1
ϕ_3	.	$\mathbf{3}$	1	1
ϕ_{ab}	.	$\mathbf{3}$.	1	5	.	4
ϕ_{N_1}	.	$\mathbf{3}$	4	5
ϕ_{N_2}	.	$\mathbf{3}$	4	5	5	.	.	.
χ	.	$\mathbf{1}'$	1	1	.	.	5
ξ_{12}	1
ξ_{23}	.	.	1	.	5	.	4
ξ_M	1
Driving Fields												
S	2
D_{ab}^α	2	.	4	2
D_{ab}^β	.	.	.	1	3	2
D_{ab}^γ	4	.	2	2
D_{N_1}	3	.	.	.	2
D'_{N_2}	.	$\mathbf{1}'$	4	2	2	.	.	2
D''_{N_2}	.	$\mathbf{1}''$	4	2	2	.	.	2
A_2	.	$\mathbf{3}$	4	2
A_3	.	$\mathbf{3}$	2
$O_{2;3}$.	.	1	1	.	.	5	2
$O_{N_1;N_2}$	4	2	1	.	.	2

Table 5: The matter-, Higgs-, flavon- and driving fields. A dot means that the field is an invariant singlet under the respective symmetry. Note that the $U(1)$ symmetries will get explicitly broken to \mathbb{Z}_n symmetries by the Higgs sector.

	SU(5)	A_4	$\mathbb{Z}_2^{(a)}$	$\mathbb{Z}_2^{(b)}$	$\mathbb{Z}_6^{(a)}$	$\mathbb{Z}_6^{(b)}$	$\mathbb{Z}_6^{(c)}$	$\mathbb{Z}_6^{(d)}$	$\mathbb{Z}_6^{(e)}$	$U(1)_a$	$U(1)_b$	$U(1)_R$
Φ_1	$\bar{5}$	4	2	5	.	.	2	1
Φ_2	$\bar{5}$	4	2	5	5	.	2	1
Φ_3	$\bar{5}$.	1	.	1	2	2
Φ_4	.	3	.	.	2	.	4	2
Φ_5	.	3	4	2	.	.	.	2
Φ_6	$\overline{45}$	4	5	.	.	1	-1	1
Φ_7	5	2	1	.	.	.	-2	1
Φ_8	5	3	.	.	1	4	2	.	.	1	.	2
Φ_9	$\overline{10}$.	.	.	5	.	2	.	.	-1	2	1
Φ_{10}	$\bar{5}$.	1	1	.	4	4	.	.	1	-1	1
Φ_{11}	5	.	1	1	.	2	2	.	.	.	-2	1
Φ_{12}	$\overline{10}$	3	.	1	.	.	4	.	.	.	-1	1
Φ_{13}	.	1'	.	.	2	.	4	2
Φ_{14}	.	1''	.	.	2	.	4	2
Φ_{15}	4	2
Φ_{16}	3
Φ_{17}	4	2
Φ_{18}	3
Φ_{19}	.	1'	2	2
Φ_{20}	.	.	1	1	.	.	3
Φ_{21}	.	3	1	.	3
Φ_{22}	4	4	2	2	.	.	2
Φ_{23}	4	2	2	.	.	2
Φ_{24}	4	4	2	.	.	.	2
Φ_{25}	4	2	.	.	.	2
Φ_{26}	4	2
Φ_{27}	2	2
Φ_{28}	10	4	.	.	.	1	.
Φ_{29}	2	4	4	.	.	2
Φ_{30}	.	3	2	4	.	.	.	2
Φ_{31}	5
Φ_{32}	5	3	.	1	.	4	5	.	.	1	.	2
Φ_{33}	$\overline{10}$	1''	.	1	.	.	5	.	.	-1	2	1
Φ_{34}	$\overline{10}$	1''	.	1	.	.	5	.	.	.	-1	1

Table 6: The messenger fields of the model. A dot means that the field is an invariant singlet under the respective symmetry. Note that the $U(1)$ symmetries will get explicitly broken to \mathbb{Z}_n symmetries by the Higgs sector.

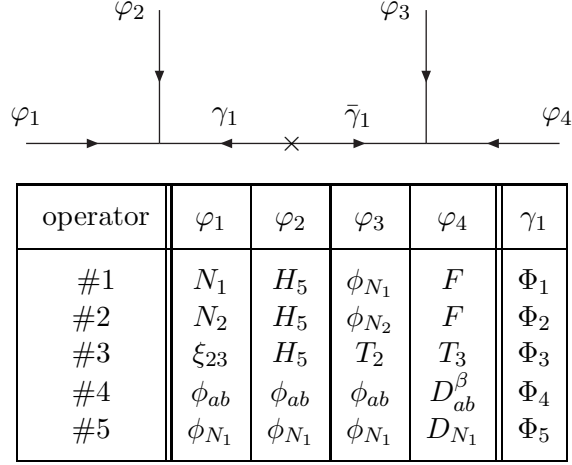


Figure 2: List of order 4 operators in the effective superpotential.

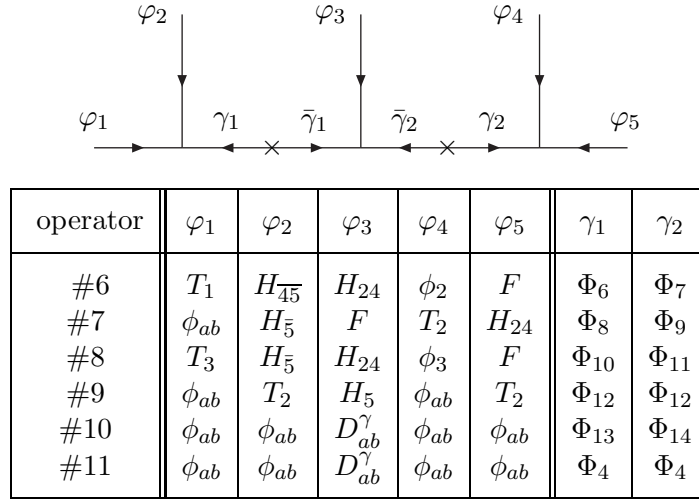


Figure 3: List of order 5 operators in the effective superpotential.

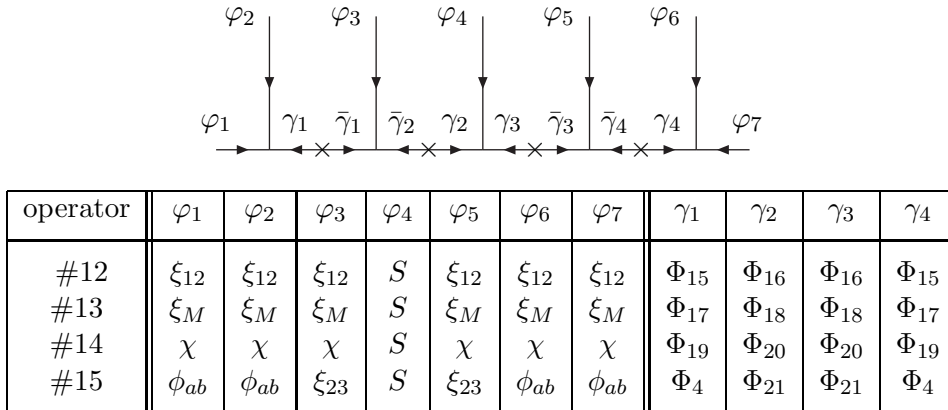


Figure 4: List of order 7 operators in the effective superpotential from supergraphs with linear topology.

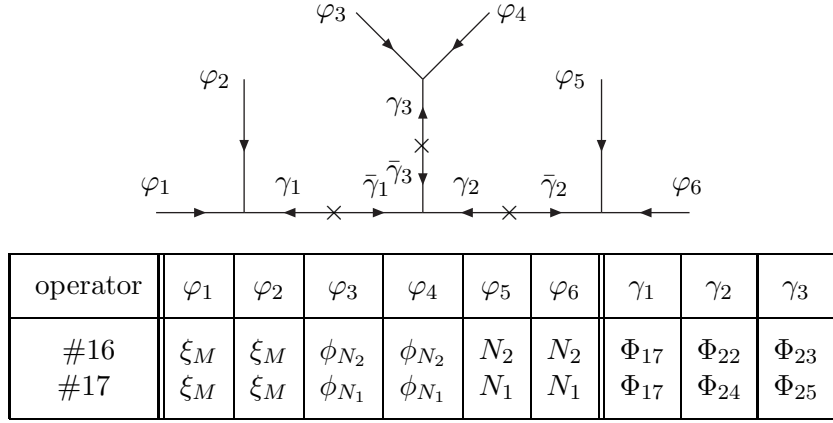


Figure 5: List of order 6 operators in the effective superpotential from supergraphs with non-linear topology.

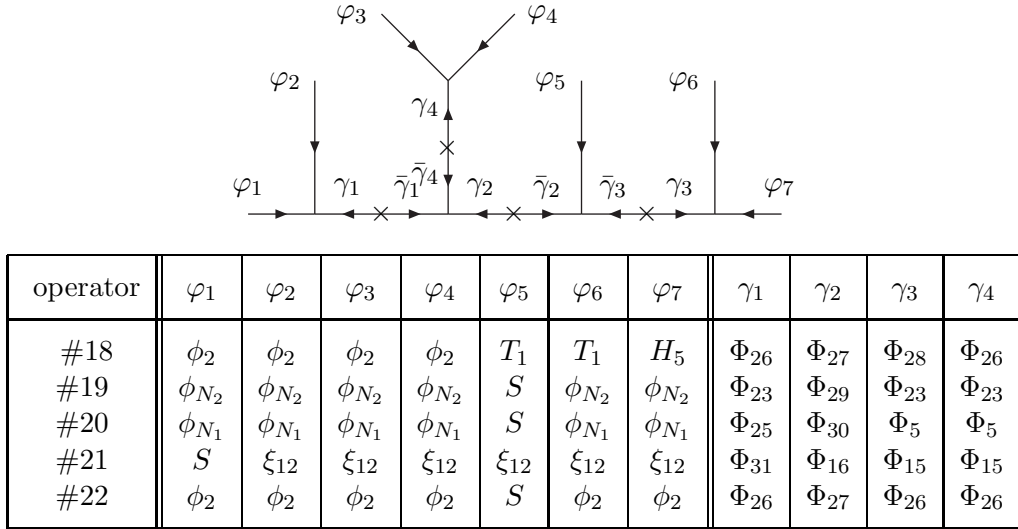


Figure 6: List of order 7 operators in the effective superpotential from supergraphs with non-linear topology.

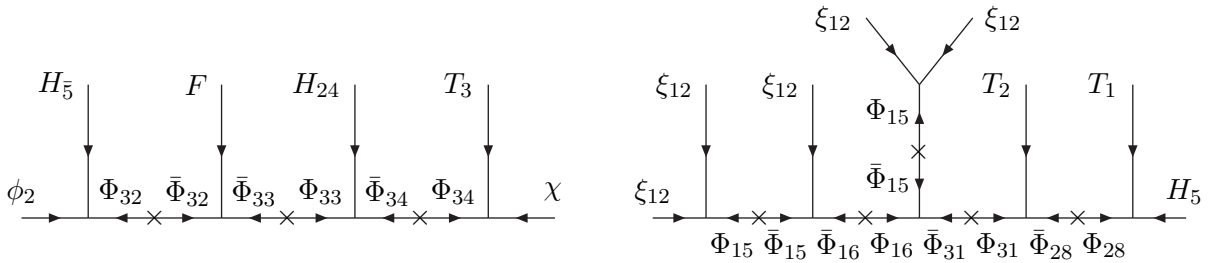


Figure 7: Additional effective operators of order 6: $[T_3 H_{24}]_{10}$ $[F H_5]_{\overline{10}}$ $\chi \phi_2$ (left) and of order 8: $T_1 T_2 \xi_{12}^5 H_5$ (right).